COBEM 2021 26th International Congress of Mechanical Engineering
November 22-26, 2021, Virtual Congress, Brazil

COB-2021-1280
MOTION OF A SOLID BODY WITHIN A GRANULAR MEDIUM

Douglas Daniel de Carvalho
Nicolao Cerqueira Lima
Erick de Moraes Franklin
School of Mechanical Engineering, UNICAMP - University of Campinas, Rua Mendeleyev, 200, Campinas, SP, Brazil
douglascarvalho47@gmail.com; nicolaolima@gmail.com; franklin@fem.unicamp.br

Abstract. *This work consists of numerical simulations of a cylindrical intruder (disk) pulled at a constant speed in a two-dimensional assembly of smaller bidisperse disks in a rectangular confining cell, so that the intruder and the grains have relative displacements. The simulations were carried out with the Discrete Element Method (DEM) using the open source software LIGGGHTS. Different physical configurations are analyzed by varying some important physical parameters of the problem, such as the speed at which the intruder is pulled. We present quantitative measurements of the force experienced by the intruder in different physical configurations, as well as an analysis of the evolution of contact and force networks (associated with the stress distribution). In addition, parameters associated with force anisotropy are also measured, such as the mean contact number and contact anisotropy. We noticed strong fluctuations in the intruder's force signal that are clearly associated with the dynamics of the force chains within the grains, which proved to be somewhat isotropic.*

Keywords: *intruder, granular media, force chains, anisotropy, DEM simulations.*

1. INTRODUCTION

The motion of a solid intruder in granular media is commonly found in nature and in various human activities. To cite just a few examples, the motion of animals and machines on and within granular matter (snakes, worms and tanks), the penetration and impact of solid objects in sand (such as ballistic objects), and the collision of objects on sandy surfaces (such as the landing of space probes on other planets) (Askari and Kamrin, 2016; Zheng *et al.*, 2018). Depending on the type of application, the intruder may experience different phenomena. For instance, its kinetic energy can be dissipated through the generated collisions in the grains (Bester and Behringer, 2017) (such as happens in ballistic impacts) and it can be subjected to stick-slip dynamics (Tordesillas *et al.*, 2014; Kozlowski *et al.*, 2019; Carlevaro *et al.*, 2020).

In the light of the complex constitutive behavior of granular media, partly due to its non-linearity, history-dependence and non-locality, forces on arbitrarily shaped granular intruders have been described by simple and yet empirical "resistive force hypotheses" (RFT) (Askari and Kamrin, 2016). The resisting force against the motion of the intruder is represented by a simple superposition principle (Maladen *et al.*, 2011), where the intruder's boundary is divided into differential elements and the total force equals the sum of the forces on each element as if it were moving on its own.

One important aspect of granular media is the formation of forces and stresses networks (force chains) under the action of external stresses. Because granular matter is a discrete medium, inter-particle forces are transmitted via a history-dependent contact network, which then forms an inhomogeneous distribution of filamentary force chains (Majmudar and Behringer, 2005). Such forces are only transmitted through the inter-particle contacts, which leads to a strong anisotropic distribution of stresses (Radjai *et al.*, 1998). Understanding these forces and their spatial correlations is one of the main goals of granular mechanics, since it is important for understanding jamming, shear-induced yielding and mechanical response (Majmudar and Behringer, 2005). If a system starts from a stress-free configuration and is subjected to increasing amounts of shear strain, it evolves from a fragile state (Cates *et al.*, 1998) into a jammed one, by altering the way the anisotropic force and contact networks percolate among the boundaries and, if shear strain continues to be applied past the point of shear jamming, the system tends to become more isotropic (Behringer *et al.*, 2013; Bi *et al.*, 2011). When intruders are set to motion in granular media, the force networks generated along the intruder-granular interface fluctuate rapidly in space and time (Clark *et al.*, 2014). As a consequence, an intruder's motion in granular media might create jamming, because cohesionless granular materials tend to form jammed states when stresses are applied (Bi *et al.*, 2011). In addition, the motion of an intruder leads to local reorganizations of the granular packing (Kolb *et al.*, 2013), leading to the breaking and local reformation of the force networks around it. One way to observe contact forces distributions is by using photoelastic techniques, making use of photoelastic (birefringent under strain) disks (Majmudar and Behringer,

2005; Daniels *et al.*, 2017). These can also be easily accessed through numerical techniques (Herman, 2016).

For the case of an intruder being pulled or pushed through a granular medium, the movement is generally accomplished in two main ways: (i) the intruder is moved at a constant speed (Albert *et al.*, 1999, 2001; Geng and Behringer, 2005; Stone *et al.*, 2004; Soller and Koehler, 2007; Costantino *et al.*, 2008; Kolb *et al.*, 2013; Seguin *et al.*, 2016; Carlevaro *et al.*, 2020; Kozlowski *et al.*, 2019; Seguin *et al.*, 2011) or (ii) it is moved at a constant force (Reichhardt and Reichhardt, 2010; Candelier and Dauchot, 2009, 2010). Although extensively studied, the physics behind the dynamics of these motions still remains poorly understood and important issues remain to be further investigated: (i) the evolution of contact and force networks; (ii) the occurrence of jamming and blockages within grains, and; (iii) displacement rates of grains. To this end, this work consists of numerical simulations of a cylindrical intruder (disk) pulled at a constant speed in a two-dimensional assembly of smaller bidisperse disks in a rectangular confining cell, so that the intruder and the grains have relative displacements. The simulations are carried out with the Discrete Element Method (DEM) using the open source software LIGGGHTS. We use exactly the same physical configuration as the one in Seguin *et al.* (2016), and validate our numerical code by replicating some of the experimental results obtained in the aforementioned paper. Finally, we present quantitative measurements of the force experienced by the intruder in different physical configurations. In addition, parameters associated with force anisotropy are also presented, such as the mean contact number and contact anisotropy.

2. NUMERICAL SETUP

The numerical simulations consist in pulling an intruder (solid disk) into a two-dimensional assembly of smaller disks. The $d_i = 16$ mm diameter and $h_i = 3.6$ mm high steel intruder is pulled at a constant velocity $10^{-1} \leq V_0 \leq 2.7$ mm/s and the granular assemble is a bidisperse mixture of 7924 photoelastic polyurethane (PSM-4) disks with small diameter $d_s = 4$ mm and large diameter $d_l = 5$ mm in order to prevent crystallization (O'Hern *et al.*, 2003). The disks with height $h_g = 3.2$ mm are distributed in a proportion of $N_l/N_s \approx 0.64$, where $N_s = 4832$ and $N_l = 3092$ are the number of small and large particles, respectively, in a way that the area occupied by the small and large grains in the simulation cell is almost the same. The disks are placed in a horizontal glass plate and are enclosed in a glass square area of $L_x \times L_y = 400 \times 400$ mm^2. All simulations are performed within a fixed cell size, in a way that the initial packing fraction of the model is kept constant at $\phi_0 = 0.76$, which is a dense packing but much smaller than the jamming packing fraction $\phi_J \approx 0.83$ (Coulais *et al.*, 2012). The physical properties of the materials used in the numerical simulations are summarized in Tab. (1).

Table 1: Physical properties of all materials used in the numerical simulations.

	Material	**Young modulus [Pa]**	**Poisson's ratio**	**Density [kg/m^3]**	**Size [mm]**
Intruder	Steel[(1)]	1.96×10^{11}	0.29	7800	$d_i = 16$
Grains	Polyurethane[(1),(2)]	4.14×10^{6}	0.50	1280	d_s = 4; d_l = 5
Walls	Glass[(1)]	0.64×10^{11}	0.23	2500	L_x = 400; L_y = 400

(1) Hashemnia and Spelt (2014)

(2) Gloss (2000)

Although the Young modulus of the steel intruder is $E = 1.96 \times 10^{11}$ Pa, we considered a smaller value in the numerical simulations of $E = 1.96 \times 10^{9}$ Pa to avoid prohibitive timesteps, without giving up the accuracy of the results (Lommen *et al.*, 2014). Since we consider pure two-dimensional simulations, no motion of both grains and intruder in the direction perpendicular to the plane xy is considered. The intruder is initially placed in the granular medium at the left side of the simulation cell at $(x_i, y_i) = (-160, 0)$ and is pulled at a constant velocity V_0 from left to right towards its final position $(x_f, y_f) = (160, 0)$, according to the scheme presented in Fig. (1). Thus, independent of the initial velocity V_0 considered, the intruder always moves a total length of $\Delta S = 320$ mm. The time evolution of the drag force $F(t)$ exerted by the grains onto the intruder disk during its displacement, the forces in each grain as well as their displacements are computed every time-step. In addition, to avoid any possible boundary effects in the force results, the analyzed cell area is restricted to a central square region of interest (ROI) - green-dashed area in Fig. (1) - of size $A_{ROI} = 160 \times 160$ mm^2. It is important to bear in mind that the physical conditions used in the numerical simulations are as close as possible as the ones used in the experiments performed by Seguin *et al.* (2016).

3. DISCRETE ELEMENT METHOD (DEM)

Discrete Element Method (DEM) is an expensive numerical technique for modeling the motion and interactions (collisions) of particles at the grain scale using a Lagrangian approach (Goniva *et al.*, 2010), having been developed for over 40 years (Cundall and Strack, 1979). Although expensive due to the large number, size, and shape distribution of particles in usual granular systems, it is a popular technique because of its ability to accurately predict the behavior of granular flows (Derakhshani *et al.*, 2015).

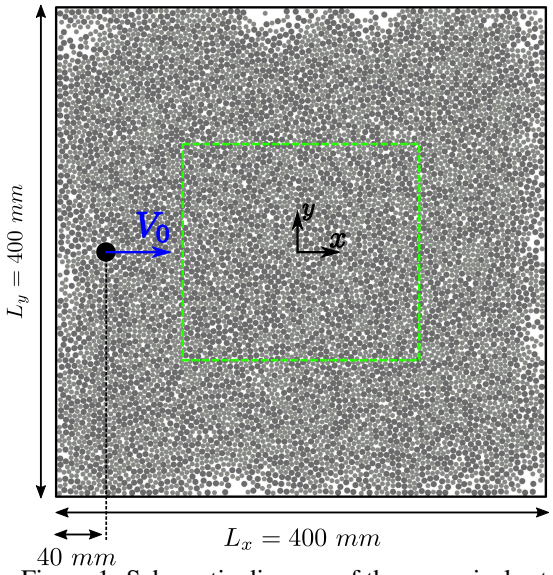

Figure 1: Schematic diagram of the numerical setup.

In this study, the simulations were carried out using LIGGGHTS (LAMMPS Improved for General Granular and Granular Heat Transfer Simulations) (Kloss *et al.*, 2012), which is a DEM open source software for modelling granular flows based on LAMMPS (Large Atomic and Molecular Massively Parallel Simulator), an open source Molecular Dynamics (MD) code by Sandia National Laboratories (Goniva *et al.*, 2010). In conjunction with LIGGGHTS, we make use of the two-dimensional Discrete-Element bonded-particle Sea Ice model - DESIgn (Herman, n.d.), a freely available toolbox suitable for use with LIGGGHTS, which, although developed for modeling sea ice problems, can be readily applied to other two-dimensional disk-shaped grains (Herman, 2016). Even though it is possible to carry out two-dimensional simulations using solely LIGGGHTS, the use of the DESIgn toolbox is extremely important, as, in general, simulations carried out with LIGGGHTS consider spherical rather than cylindrical (disk) particles, as is the case with the particles in our work. Thus, even if two-dimensional simulations are performed using purely LIGGGHTS, the results obtained would be physically inconsistent, due to the erroneous shape of the particles. According to Herman (2016), the essential difference between spherical and cylindrical objects in contact is the shape of their contact surface, which is circular for two spherical particles in contact and rectangular for two cylindrical particles in contact. It it also important to mention that the DESIgn toolbox only works in older versions of LIGGGHTS, which is currently in its 3.8.0 version. In this way, the numerical simulations performed in this work were all carried out using LIGGGHTS 3.1.0.

3.1 Contact model

In this section, we present the mathematical modeling used by LIGGGHTS in conjunction with the DESIgn toolbox for computing the particles dynamics. For a complete description of the modeling, please refer to Herman (2016) and (Derakhshani *et al.*, 2015).

For the case of N disk-shaped grains, each with a constant mass $m_i = \rho_i h_i \pi r_i^2$ for $i = 1 \cdots N$, their motion can only be influenced by: (i) the particle-particle and particle-wall interaction forces, and (ii) other external forces. For simplicity, the particle-wall forces will not be included in the equations below, since they are modeled in the exact same way as the particle-particle interactions. For each particle $j \in N$ in contact with particle i, there exists a contact force $\mathbf{F}_{c,ij}$ which is conveniently expressed as the sum of two components, normal $\mathbf{F}_{c,ij,n}$ and tangential $\mathbf{F}_{c,ij,t}$ to the plane of contact. The normal component contributes to the translational motion of disks i and j and the tangential component the their rotational motion. This way, the torque $\mathbf{M}_{c,ij}$ due to the tangential forces may be expressed as (Herman, 2016):

$$\mathbf{M}_{c,ij} = \mathbf{r}_{ij} \times \mathbf{F}_{c,ij,t}, \tag{1}$$

where $\mathbf{r}_{ij}$ is a vector pointing from the center of disk i with center position vector $\mathbf{x}_i = (x_i, y_i, z_i = 0)$ to the contact point with disk j. Once again, it is important to mention that this is a two-dimensional problem, which precisely means that $z_i = 0$.

The motion of all grains is governed by Newton's second law of motion. Therefore, the translational and rotational motions of particle i, in contact with grains $j \in \mathcal{C}$, where $\mathcal{C}$ denotes all particles in contact with grain i, are given by:

$$m_i \frac{d\mathbf{u}_i}{dt} = \sum_{j \in \mathcal{C}} \mathbf{F}_{c,ij} + \mathbf{F}_e, \tag{2}$$

where t denotes time, $\mathbf{u}_i = (u_{x,i}, u_{y,i}, u_{z,i} = 0)$ is the velocity vector of particle i, and $\mathbf{F}_e$ is the sum of all external forces acting on particle i, and,

$$I_{z,i}\frac{d\omega_{z,i}}{dt} = M_{c,ij} + M_e, \tag{3}$$

where $I_{z,i} = (1/2)m_i r_i^2$ is the moment of inertia, $\omega_{z,i}$ is the angular velocity of particle i, $M_{c,ij}$ is the net moment generated by the tangential contact forces and M_e is the net moment of the external forces.

Although there are no explicit external forces acting on our system, since we are dealing with dry granular media, the DESIgn toolbox does not consider the sliding frictional force that exists between the grains/intruder and the bottom glass wall on which they are placed. Therefore, we had to implement a new force to account for the effects of an effective solid friction between the grains/intruder and the base into the library of the DESIgn toolbox. This force was modeled in a similar manner to what has been done in Carlevaro *et al.* (2020). In short, if a grain i is moving at a certain velocity $v_i = |\mathbf{u}_i|$ above a threshold v' ($v_i > v'$), then a dynamic friction force with the bottom wall is considered and equal to $F_d = -\mu_{d,g} m_i g \mathbf{u}_i/|\mathbf{u}_i|$. Conversely, if it is moving with a velocity v_i smaller than or equal to the threshold v' ($v_i \leq v'$), then an static friction force with the bottom wall $F_s = -\mu_{s,g} m_i g \mathbf{u}_i/|\mathbf{u}_i|$ is applied and the particle is immobilized by setting $v_i = 0$. This ensures that a grain will only resume its motion if the forces exerted by the other grains exceed the static friction force (Carlevaro *et al.*, 2020). In this model, we do not consider rotational friction forces between the grains and the bottom wall.

As for modeling the contact forces, the nonlinear elastic Hertz-Mindlin contact model, appropriate for non-cohesive interactions, is used. This model consists in the combination of two spring-dashpots, the first one undertaking the normal interactions and a Coulomb friction coefficient μ for shear interactions and the second spring-dashpot undertaking the tangential forces (Derakhshani *et al.*, 2015). At each time step, the magnitude of the tangential force is limited through the Coulomb friction law (Herman, 2016):

$$|\mathbf{F}_{c,ij,t}| \leq \mu |\mathbf{F}_{c,ij,n}|, \tag{4}$$

where μ is static yield criterion.

In this scenario, the normal $\mathbf{F}_{c,ij,n}$ and tangential $\mathbf{F}_{c,ij,t}$ forces can be decomposed as the sum of two terms. Their magnitude are given, respectively, by (Herman, 2016):

$$F_{c,n} = \kappa_n \delta_n - \gamma_n \frac{d\delta_n}{dt} \tag{5}$$

$$F_{c,t} = \kappa_t \delta_t - \gamma_t \frac{d\delta_t}{dt} \tag{6}$$

The two normal forces in Eq. (5) are a repulsive and a viscoelastic damping force. As for the case of Eq. (6), the tangential force is the sum of a shear and a damping force. In Equations (5) and (6), δ_n is the normal displacement and $\delta_n \geq 0$ when two grains are in contact; δ_t is the tangential displacement, measured in the direction perpendicular to the plane of contact, accounting for the "history" effects of the contact. In addition, the coefficients κ_n, κ_t, γ_n, and γ_t are functions of the displacements as well of the shape, size and material properties of the particles in contact. The exact form of such coefficients depend on the contact model chosen. All damping components depend on the relative velocity between the interacting particles. One notices that $d\delta_n/dt$ denotes the normal and $d\delta_t/dt$ denotes the tangential component of the relative velocity of the interacting particles (Herman, 2016).

For the case of two interacting particles i and j, characterized by Young moduli E_i and E_j, Poisson's ratios ν_i and ν_j, radii r_i and r_j and thickness h_i and h_j, with $h_m = \min\{h_i, h_j\}$, one can define an effective radius r_c, an effective mass m_c, an effective contact modulus E_c and an effective shear modulus G_c as:

$$r_c = \frac{r_i r_j}{r_i + r_j}; \qquad m_c = \frac{m_i m_j}{m_i + m_j}, \tag{7}$$

$$E_c = \left(\frac{1-\nu_i^2}{E_i} + \frac{1-\nu_j^2}{E_j}\right)^{-1}; \qquad G_c = \frac{1}{2}\left[\frac{(1-\nu_i)(2+\nu_i)}{E_i} + \frac{(1-\nu_j)(2+\nu_j)}{E_j}\right]^{-1} \tag{8}$$

In addition, the normal overlap (displacement) δ_n between the disks in contact is measured along $\mathbf{r}_{ij}$ and is defined as:

$$\delta_n = r_i + r_j - |\mathbf{x}_i - \mathbf{x}_j| \tag{9}$$

The equations presented above are also valid if one of the materials in contact is a wall, as already mentioned. In this case, for a flat wall, $r_j \to \infty$, δ_n is calculated using the normal distance of the grain to the wall, and δ_t is calculated as the displacement of the grain's center parallel to the wall (Herman, 2016).

Some contact modes also relate the damping ratio β with the restitution coefficient ϵ for underdamped systems, leading to:

$$\beta = \frac{\ln(\epsilon)}{\sqrt{\ln^2(\epsilon) + \pi^2}} \tag{10}$$

For the case of two elastic cylinders, the normal displacement is given by (Herman, 2016):

$$\delta_n = \frac{F_{c,n}}{\pi h_m E_c}\left[1 + \ln\left(\frac{2\pi h_m^3 E_c}{r_c F_{c,n}}\right)\right] \tag{11}$$

After some algebra, an approximate expression for the normal contact force is obtained (Herman, 2016):

$$F_{c,n} = \pi E_c h_m \delta_n f\left(\frac{\delta_n r_c}{2h_m^2}\right), \tag{12}$$

this way, κ_n in Eq. (5) is defined as:

$$\kappa_n = \pi E_c h_m f\left(\frac{\delta_n r_c}{2h_m^2}\right); \qquad f(x) = \frac{p_1 x^2 + p_2 x + p_3}{x^2 + q_1 x + q_2} \tag{13}$$

In the modeling, a rational expression for f is used in in the DESIgn toolbox, as denoted by the second expression in the right side of Eq. (13), whose coefficients for $x \in [0, 0.2]$ are: $p_1 = 0.9117$, $p_2 = 0.2722$, $p_3 = 0.003324$, $q_1 = 1.524$, and $q_2 = 0.03159$ (Herman, 2016).

In many viscoelastic contact models, the Hertzian theory is used to calculate the normal repulsive force (i.e., the κ_n coefficient), as well as to estimate the shear and damping terms in Eqs. (5) and (6). In the DESIgn toolbox, κ_n is calculated from Eq. (13) and the remaining coefficients by (Herman, 2016):

$$\kappa_t = 6\frac{G_c}{E_c}\kappa_n; \qquad \gamma_n = -\beta\sqrt{5\kappa_n m_c}; \qquad \gamma_t = -2\beta\sqrt{5\frac{G_c}{E_c}\kappa_n m_c} \tag{14}$$

3.2 Numerical time step

The equations of motion presented in section 3.1 are numerically integrated in time using the energy-conserving velocity Verlet solver, that takes into account the position as well as the the linear and angular velocities of the particles (Herman, 2016). A sufficient short numerical time step is recommended to be used due to numerical stability and accuracy of the DEM simulation. To this end, Rayleigh (Δt_R) and Hertz (Δt_H) times are implemented in the DEM code and are periodically calculated during the simulation (Derakhshani *et al.*, 2015). The expressions for the Rayleigh and Hertz times are (Kloss *et al.*, 2012):

$$\Delta t_R = \frac{\pi r\sqrt{\rho/G}}{0.163\nu + 0.8766}; \qquad \Delta t_H = 2.87\left(\frac{m^2}{rE^2 V_{max}}\right)^{0.2} \tag{15}$$

It is recommended that the DEM time step is kept at a fraction of these values. All of our simulations were performed with a time step $\Delta t = 3.2 \times 10^{-6}$ s, which, in the worst scenario, leads to $\Delta t \approx 0.016\Delta t_R$, assuring the stability and accuracy of the results obtained.

3.3 Code initialization and validation

After determining the physical configuration to be studied, the set of particles with the aimed proportion is generated. First, the particles are randomly distributed over a space larger than the wanted computational domain. Then, the computational domain is compressed to its final size so that the desired packing fraction ϕ is achieved, according to Eq. (16) (Kolb *et al.*, 2013).

$$\phi = \frac{\frac{\pi}{4}(N_s d_s^2 + N_l d_l^2)}{L_x L_y - \frac{\pi}{4} d_i^2} \tag{16}$$

The particles are then allowed to relax for a sufficient time until no internal stresses are observed. Once the fully relaxed state is reached, the intruder is set in motion at a constant speed, as described in section 2.

It is important to mention again that this is a purely numerical work, whose results were obtained through the open source software LIGGGHTS in conjunction with the DESIgn toolbox (section 3). Thus, due to the absence of experimental results under the physical conditions studied, we made use of some of the experimental results obtained by Seguin *et al.* (2016), in order to validate our results obtained numerically. To do so, we simulated the same physical conditions studied by Seguin *et al.* (2016) and compared the results obtained by us numerically and by them experimentally. Similar to what was presented in Seguin *et al.* (2016), we studied the mean force experienced by the intruder as a function of its constant displacement velocity, as presented in Fig. (2).

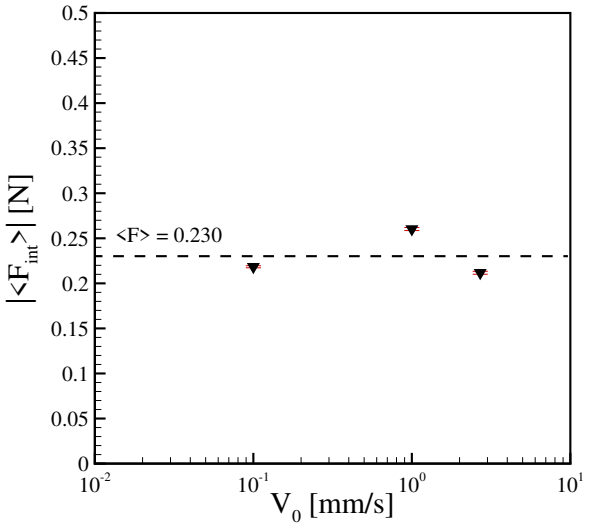

Figure 2: Mean intruder force as a function of its displacement velocity. Results obtained with the parameters described in Tab. (2).

As indicated in Fig. (2), we studied three distinct intruder velocities: $V_0 = 0.1, 1.0$ and 2.7 mm/s. One notices that for the range of V_0 studied, the mean force experienced by the intruder $< F >$ is roughly constant, in agreement with the experimental results obtained by Seguin *et al.* (2016), which has obtained an average of $< F >= 0.22$ N over their entire V_0 range, which ranged from $10^{-4} \leq V_0 \leq 2.7$ mm/s. In our case, we obtained an average of $< F >= 0.230$ N, which is very close to the results obtained by Seguin *et al.* (2016). The condition $< F > \approx$ constant with variations on V_0 is also reported on other works (Seguin *et al.*, 2011; Albert *et al.*, 1999, 2001).

We also compared the grain's velocity field generated by the intruder's movement and observed the same qualitative behavior reported in Seguin *et al.* (2016), such as the presence of a recirculation zone and that the disturbances generated by the intruder's movement are strongly located in its vicinity. We decided not to present these results here due to size restrictions. In this way, due to the similarity between the results obtained by us numerically and those obtained experimentally in Seguin *et al.* (2016), it was possible to validate our numerical code, so that it can be used to study different physical conditions, sometimes difficult to be carried out experimentally, in addition to the possibility of extracting physical quantities that are difficult to measure experimentally.

In addition, the influence of the variation of ten physical parameters inherent to the numerical model on the force experienced by the intruder was fully mapped. The values of the final coefficients that account for the results are given in Tab. (2).

4. RESULTS

In this section, we present some of the numerical results obtained for the displacement of an intruder moving at a constant speed in an assembly of smaller grains, as described in sections 2and 3. Since the dynamics observed is similar for the different intruder's velocity studied, as indicated in Fig. (2), the results presented below are all for $V_0 = 2.7$ mm/s.

Figure (3a) shows the drag force $F(t)$ experienced by the intruder as a function of time t. In order to avoid any possible boundary effects, the average force was calculated in the region of interest (ROI) - green-dashed area in Fig. (1) -, whose result is depicted in Fig. (2). At first, there are strong fluctuations in the intruder's force signal (Clark *et al.*, 2014) that are clearly associated with the dynamics of the force chains within the grains, which can be either created or broken while the intruder is pulled at a constant speed (Seguin *et al.*, 2016). The peaks observed in the signal are associated with more robust force chains, which in turn tend to impede the intruder's free movement, which is pulled at a constant speed, naturally leading to an increase in its drag force. The lower force values, on the other hand, are associated with the breaking of the force chains. This result is in qualitative agreement with the force signals obtained by Seguin *et al.* (2016).

Table 2: Coefficients used in the numerical simulations.

Coefficient	**Symbol**	**Base value**
Friction coefficient (grain-grain)(1)	μ_{gg}	1.2
Friction coefficient (grain-intruder)(2)	μ_{gi}	1.8
Friction coefficient (grain-wall)(1)	μ_{gw}	0.4
Restitution coefficient (grain-grain)	ϵ_{gg}	0.3
Restitution coefficient (grain-intruder)(2)	ϵ_{gi}	0.7
Restitution coefficient (grain-wall)(3)	ϵ_{gw}	0.7
Dynamic friction coefficient (grain-bottom wall)(1)	$\mu_{d,g}$	0.4
Static friction coefficient (grain-bottom wall)	$\mu_{s,g}$	0.7
Dynamic friction coefficient (intruder-bottom wall)	$\mu_{d,i}$	0.7
Threshold velocity (dynamic/static friction)	v'	5.0×10^{-4}

(1) Carlevaro *et al.* (2020)

(2) Hashemnia and Spelt (2014)

(3) Gondret *et al.* (2002)

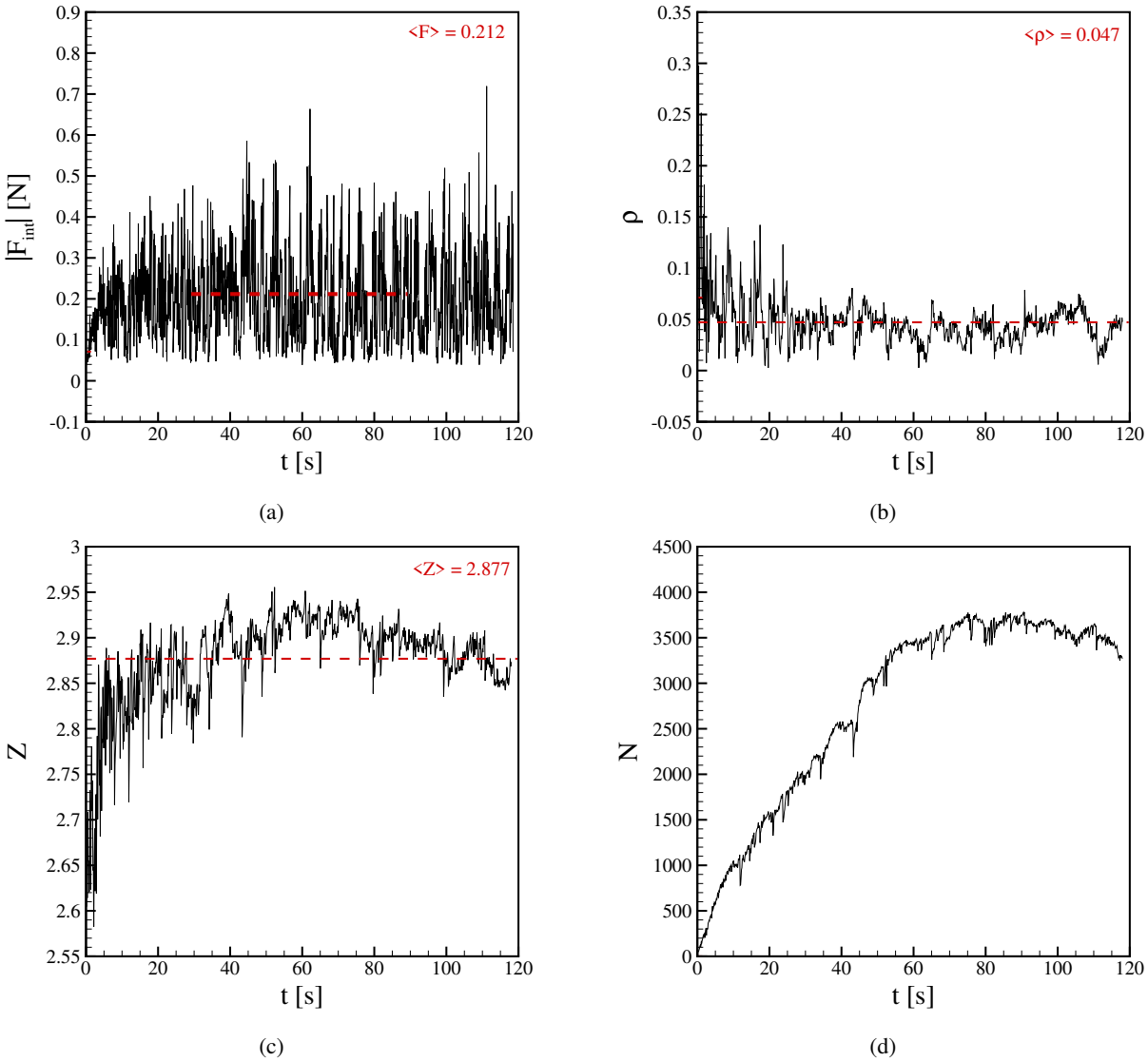

Figure 3: (a) Time evolution of the intruder's drag force $F(t)$. (b) Contact network anisotropy ρ. (c) Mean contact number per particle Z. (d) Number of non-rattler particles N. All results were obtained for the intruder's velocity $V_0 = 2.7$ mm/s.

One important aspect of granular media is the formation of a contact network (force chains) that percolates the grains, which is associated with the transmission of inter-particle forces (Majmudar and Behringer, 2005). The force chains,

generally anisotropic structures, depending on the amount shear strain, may become more isotropic (Bi *et al.*, 2011). An effective way to characterize such anisotropy is through the well-known fabric tensor $\hat{R}$ (Bi *et al.*, 2011):

$$\hat{R} = \frac{1}{N} \sum_{i \neq j} \frac{\mathbf{r}_{ij}}{|\mathbf{r}_{ij}|} \otimes \frac{\mathbf{r}_{ij}}{|\mathbf{r}_{ij}|}, \tag{17}$$

where N is the number of non-rattler particles (particles with at least two contacts), $\mathbf{r}_{ij}$ is the contact vector from the center of particle i to the contact between particles i and j and $\otimes$ denotes the vector outer product. With the eigenvalues of tensor $\hat{R}$, R_1 and R_2, it is possible to calculate the mean contact number per particle $Z = R_1 + R_2$ and the contact network anisotropy $\rho = R_1 - R_2$ (Bi *et al.*, 2011).

As indicated in Fig. (3b), the signal obtained for the contact network anisotropy ρ contains fluctuations, whose intensities are much smaller than those observed in the signal obtained for the drag force on the intruder - Fig. (3a) -, for example. Such fluctuations can be interpreted as indicative of the presence of more anisotropic force chains zones (higher values of ρ) in conjunction with more isotropic force chains zones (lower values of ρ). However, in general, despite a strong transient in the value of ρ at the beginning of the intruder's movement, the contact network anisotropy ρ is approximately constant throughout its displacement, with a mean value of $<\rho>$ = 0.047. This indicates the presence of more isotropic force chains along the intruder's full displacement, as opposed to anisotropic force chains at the beginning of the intruder's movement.

As for the mean contact number per particle Z, it can be seen in Fig. (3c) that it tends to increase in the first seconds of the intruder's displacement until it reaches an approximately constant value of $Z = 2.877$. The mean contact number per particle Z is a key parameter for mechanical stability, and can be used to characterize jamming; however, the minimum number of contacts needed to characterize jamming conditions can cover a range of values depending on some parameters, such as the form of grains preparation (Bi *et al.*, 2011). According to Majmudar *et al.* (2007), a reasonable criterion for isotropic jamming is $Z \geq 3.0$ to $Z \approx 3.1$, which is a higher value than what we obtained ($Z \approx 2.88$), thus characterizing non-jammed regions along the intruder's entire displacement, even though local-jammed regions might appear, especially in regions in front of the intruder. This was somewhat expected, since we consider an initial packing fraction $\phi_0 = 0.76$, which is much smaller than the jamming packing fraction $\phi_J \approx 0.83$.

Finally, Fig. (3d) depicts the number of non-rattler particles N as a function of time t. It is clear that N tends to increase with t until it saturates at around $N \approx 3800$. This indicates that the compression exerted by the intruder on the grains as it moves tends to push them towards the right wall, generating an increase in the number of particles that are in contact. As the space for particles to move tends to decrease as the intruder gets closer to the wall, there is an increase in the concentration of grains that tend to get closer and closer to the wall, thus causing the number of particles with at least two contacts to increase.

5. ACKNOWLEDGEMENTS

The authors are grateful to FAPESP (Grant numbers 2018/14981-9, 2019/20888-2 and 2020/04151-7) for the financial support provided.

6. REFERENCES

Albert, I., Sample, J., Morss, A., Rajagopalan, S., Barabási, A.L. and Schiffer, P., 2001. "Granular drag on a discrete object: Shape effects on jamming". *Physical review E*, Vol. 64, No. 6, p. 061303.

Albert, R., Pfeifer, M., Barabási, A.L. and Schiffer, P., 1999. "Slow drag in a granular medium". *Physical review letters*, Vol. 82, No. 1, p. 205.

Askari, H. and Kamrin, K., 2016. "Intrusion rheology in grains and other flowable materials". *Nature materials*, Vol. 15, No. 12, pp. 1274–1279.

Behringer, R., Dijksman, J., Ren, J., Zhang, J., Majmudar, T., Chakraborty, B., Bi, D. and Tordesillas, A., 2013. "Jamming and shear for granular materials". In *AIP Conference Proceedings*. American Institute of Physics, Vol. 1542, pp. 12–19.

Bester, C.S. and Behringer, R.P., 2017. "Collisional model of energy dissipation in three-dimensional granular impact". *Physical Review E*, Vol. 95, No. 3, p. 032906.

Bi, D., Zhang, J., Chakraborty, B. and Behringer, R.P., 2011. "Jamming by shear". *Nature*, Vol. 480, No. 7377, pp. 355–358.

Candelier, R. and Dauchot, O., 2009. "Creep motion of an intruder within a granular glass close to jamming". *Physical review letters*, Vol. 103, No. 12, p. 128001.

Candelier, R. and Dauchot, O., 2010. "Journey of an intruder through the fluidization and jamming transitions of a dense granular media". *Physical Review E*, Vol. 81, No. 1, p. 011304.

Carlevaro, C.M., Kozlowski, R., Pugnaloni, L.A., Zheng, H., Socolar, J.E. and Kondic, L., 2020. "Intruder in a two-

dimensional granular system: Effects of dynamic and static basal friction on stick-slip and clogging dynamics". *Physical Review E*, Vol. 101, No. 1, p. 012909.

Cates, M., Wittmer, J., Bouchaud, J.P. and Claudin, P., 1998. "Jamming, force chains, and fragile matter". *Physical review letters*, Vol. 81, No. 9, p. 1841.

Clark, A.H., Petersen, A.J. and Behringer, R.P., 2014. "Collisional model for granular impact dynamics". *Physical review E*, Vol. 89, No. 1, p. 012201.

Costantino, D., Scheidemantel, T., Stone, M.B., Conger, C., Klein, K., Lohr, M., Modig, Z. and Schiffer, P., 2008. "Starting to move through a granular medium". *Physical review letters*, Vol. 101, No. 10, p. 108001.

Coulais, C., Behringer, R. and Dauchot, O., 2012. "Dynamics of the contacts reveals widom lines for jamming". *EPL (Europhysics Letters)*, Vol. 100, No. 4, p. 44005.

Cundall, P.A. and Strack, O.D., 1979. "A discrete numerical model for granular assemblies". *geotechnique*, Vol. 29, No. 1, pp. 47–65.

Daniels, K.E., Kollmer, J.E. and Puckett, J.G., 2017. "Photoelastic force measurements in granular materials". *Review of Scientific Instruments*, Vol. 88, No. 5, p. 051808.

Derakhshani, S.M., Schott, D.L. and Lodewijks, G., 2015. "Micro–macro properties of quartz sand: experimental investigation and dem simulation". *Powder Technology*, Vol. 269, pp. 127–138.

Geng, J. and Behringer, R.P., 2005. "Slow drag in two-dimensional granular media". *Physical review E*, Vol. 71, No. 1, p. 011302.

Gloss, K.T., 2000. *A Photoelastic Investigation Into The Effects Of Cracks And Boundary Conditions On Stress Intensity Factors In Bonded Specimens*. Ph.D. thesis, Virginia Tech.

Gondret, P., Lance, M. and Petit, L., 2002. "Bouncing motion of spherical particles in fluids". *Physics of fluids*, Vol. 14, No. 2, pp. 643–652.

Goniva, C., Kloss, C., Hager, A. and Pirker, S., 2010. "An open source CFD-DEM perspective". In *Proceedings of OpenFOAM Workshop, Göteborg*. pp. 22–24.

Hashemnia, K. and Spelt, J.K., 2014. "Particle impact velocities in a vibrationally fluidized granular flow: measurements and discrete element predictions". *Chemical Engineering Science*, Vol. 109, pp. 123–135.

Herman, A., 2016. "Discrete-element bonded-particle sea ice model DESIgn, version 1.3 a–model description and implementation". *Geoscientific Model Development*, Vol. 9, No. 3, pp. 1219–1241.

Herman, A., n.d. "DESIgn - discrete-element bonded-particle sea ice model". Institute of Oceanography, University of Gdańsk, https://herman.ocean.ug.edu.pl/LIGGGHTSseaice.html. Accessed 16 june 2021.

Kloss, C., Goniva, C., Hager, A., Amberger, S. and Pirker, S., 2012. "Models, algorithms and validation for opensource DEM and CFD–DEM". *Progress in Computational Fluid Dynamics, an International Journal*, Vol. 12, No. 2-3, pp. 140–152.

Kolb, E., Cixous, P., Gaudouen, N. and Darnige, T., 2013. "Rigid intruder inside a two-dimensional dense granular flow: Drag force and cavity formation". *Physical Review E*, Vol. 87, No. 3, p. 032207.

Kozlowski, R., Carlevaro, C.M., Daniels, K.E., Kondic, L., Pugnaloni, L.A., Socolar, J.E., Zheng, H. and Behringer, R.P., 2019. "Dynamics of a grain-scale intruder in a two-dimensional granular medium with and without basal friction". *Physical Review E*, Vol. 100, No. 3, p. 032905.

Lommen, S., Schott, D. and Lodewijks, G., 2014. "DEM speedup: Stiffness effects on behavior of bulk material". *Particuology*, Vol. 12, pp. 107–112.

Majmudar, T.S. and Behringer, R.P., 2005. "Contact force measurements and stress-induced anisotropy in granular materials". *Nature*, Vol. 435, No. 7045, pp. 1079–1082.

Majmudar, T., Sperl, M., Luding, S. and Behringer, R.P., 2007. "Jamming transition in granular systems". *Physical review letters*, Vol. 98, No. 5, p. 058001.

Maladen, R.D., Ding, Y., Umbanhowar, P.B., Kamor, A. and Goldman, D.I., 2011. "Mechanical models of sandfish locomotion reveal principles of high performance subsurface sand-swimming". *Journal of The Royal Society Interface*, Vol. 8, No. 62, pp. 1332–1345.

O'Hern, C.S., Silbert, L.E., Liu, A.J. and Nagel, S.R., 2003. "Jamming at zero temperature and zero applied stress: The epitome of disorder". *Physical Review E*, Vol. 68, No. 1, p. 011306.

Radjai, F., Wolf, D.E., Jean, M. and Moreau, J.J., 1998. "Bimodal character of stress transmission in granular packings". *Physical review letters*, Vol. 80, No. 1, p. 61.

Reichhardt, C.O. and Reichhardt, C., 2010. "Fluctuations, jamming, and yielding for a driven probe particle in disordered disk assemblies". *Physical Review E*, Vol. 82, No. 5, p. 051306.

Seguin, A., Coulais, C., Martinez, F., Bertho, Y. and Gondret, P., 2016. "Local rheological measurements in the granular flow around an intruder". *Physical Review E*, Vol. 93, No. 1, p. 012904.

Seguin, A., Bertho, Y., Gondret, P. and Crassous, J., 2011. "Dense granular flow around a penetrating object: Experiment and hydrodynamic model". *Physical review letters*, Vol. 107, No. 4, p. 048001.

Soller, R. and Koehler, S., 2007. "Random fluctuations and oscillatory variations of drag forces on vanes rotating in

granular beds". *EPL (Europhysics Letters)*, Vol. 80, No. 1, p. 14004.

Stone, M., Barry, R., Bernstein, D., Pelc, M., Tsui, Y. and Schiffer, P., 2004. "Local jamming via penetration of a granular medium". *Physical Review E*, Vol. 70, No. 4, p. 041301.

Tordesillas, A., Hilton, J.E. and Tobin, S.T., 2014. "Stick-slip and force chain evolution in a granular bed in response to a grain intruder". *Physical Review E*, Vol. 89, No. 4, p. 042207.

Zheng, H., Wang, D., Chen, D.Z., Wang, M. and Behringer, R.P., 2018. "Intruder friction effects on granular impact dynamics". *Physical Review E*, Vol. 98, No. 3, p. 032904.

7. RESPONSIBILITY NOTICE

The authors are solely responsible for the printed material included in this paper.